REPORT DOCUMENTATION PAGE

Public reporting burden for this collection of information is estimated to average 1 hour per response, including the time for reviewing instructions, searching existing data sources, gathering and maintaining the data needed, and completing and reviewing the collection of information. Send comments regarding this burden estimate or any other aspect of this collection of information, including suggestions for reducing this burden, to Washington Headquarters Services, Directorate for Information Operations and Reports, 1215 Jefferson Davis Highway, Suite 1204, Arlington, VA 22202-4302, and to the Office of Management and Budget, Paperwork Reduction Project (0704-0188), Washington, DC 20503.

1. AGENCY USE ONLY (Leave blank)	2. REPORT DATE	3. REPORT TYPE AND DATES COVERED
	16 January 1998	Final Report, 1 Mar 95 - 28 Feb 97

4. TITLE AND SUBTITLE

Final Report on "Multiple Scatter Theory of Ocean Sediments II," under Grant N00014-95-1-0536, for the period 1 Mar 95 - 28 Feb 97

5. FUNDING NUMBERS

6. AUTHOR(S)

Dr. Nicholas P. Chotiros

7. PERFORMING ORGANIZATION NAMES(S) AND ADDRESS(ES)

Applied Research Laboratories
The University of Texas at Austin
P.O. Box 8029
Austin, Texas 78713-8029

8. PERFORMING ORGANIZATION REPORT NUMBER

9. SPONSORING/MONITORING AGENCY NAME(S) AND ADDRESS(ES)

Jeffrey Simmen, ONR321OA
Office of Naval Research, Office of the Navy
Ballston Tower One
800 North Quincy Street
Arlington, VA 22217-5660

10. SPONSORING/MONITORING AGENCY REPORT NUMBER

11. SUPPLEMENTARY NOTES

12a. DISTRIBUTION/AVAILABILITY STATEMENT

Approved for public release;
distribution unlimited.

12b. DISTRIBUTION CODE

13. ABSTRACT (Maximum 200 words)

To support research in understanding the mechanism of the wave attenuation and scattering in the porous media composed of granual material. The parameters to be controlled are sediment grain size, surface roughness, and gas content.

14. SUBJECT TERMS

15. NUMBER OF PAGES

16. PRICE CODE

17. SECURITY CLASSIFICATION OF REPORT	18. SECURITY CLASSIFICATION OF THIS PAGE	19. SECURITY CLASSIFICATION OF ABSTRACT	20. LIMITATION OF ABSTRACT
Unclassified	Unclassified	Unclassified	

Final Report

Title: Multiple scatter theory of ocean sediments II

Principal Investigator: Nicholas P. Chotiros

Grant: N00014-95-1-0536

Category: Bottom scattering

Address: Applied Research Laboratories, University of Texas at Austin, Texas 78713-8029

e-mail chotiros@arlut.utexas.edu, tel. (512)-835-3512, fax. (512)-835-3259

Long-term goals:

To develop a new model of acoustic bottom backscatter from sandy sediments, based on a multiple scattering theory approach, and hence, properly explain observed phenomena, including Lambert's rule and frequency dependence of backscattering strength, particularly at shallow grazing angles, for which current theories are at a loss.

Scientific or technological (S&T) objectives:

The underlying idea is based on the fact that real sediments are granular. The hypothesis to be proved is that physical mechanisms for both attenuation and scattering may be found in the interaction of acoustic waves with the granular structure.

Accomplishments:

The effects of granularity have been added to a Biot model of ocean sediments in a numerical simulation by introducing homogeneous layers of random thicknesses on the order of a grain diameter, in which the mean porosity is preserved. Within each layer, conservation of grain volume dictates a linear relationship between the layer thickness, porosity, and grain diameter.

Lateral variations in sediment structure were simulated by coherently averaging the results for several random realizations of a layered poroelastic medium with given grain size and layer thickness distributions. The reflection loss predicted by this model was computed from the coherent component of the ensemble average of the reflected signal and was found to be in good

agreement with measured values by Nolle. Papers[1,2] were presented at the Spring and Fall Meetings of the Acoustical Society of America.

The scattering strength may be computed from the random component of the reflected signal and preliminary results were obtained, but further development of the scattering model was delayed by important findings in the propagation results. These findings are very relevant to the experimental efforts to detect the slow wave in sandy sediments and provide a new insight into the nature of sound propagation and scattering in sandy media. The results indicate that there is a continual process of energy conversion between the two compressional waves which changes the energy partition. At normal incidence, the results indicate that, after a couple of centimeters, the slow wave becomes undetectable. The cause is likely to be conversion of the slow wave energy into fast wave energy, since there are few other mechanisms of energy removal. The conversion takes place, not at the water-sand interface, but gradually as the sound energy propagates into the sand. This result explains why the slow wave was only detected at shallow grazing angles, and why many researchers have failed to detect the slow wave in simple point-to-point measurements and with sound beams incident on the sand at normal incidence. This result also has an impact on the scattering model because it alters the energy balance of the bottom penetrating waves. The findings are reported in Encl. (2), which is also a paper that is being submitted for publication in the Journal of the Acoustical Society of America.

Impact on S&T, or transition/integration expected:
The result will lead to a unified theory of propagation and scattering in porous media, applicable to ocean sediments over a broad range of frequencies, which will replace much of the disjointed collection of submodels currently in use, and which will properly explain the observed frequency, grain size, and grazing angle dependencies. After follow-on laboratory experimental verification, the results of this project will transition into sonar performance prediction models.

References

1. D. Yelton and N. P. Chotiros, "New multiple scatter model of the ocean sediment," J. Acoust. Soc. Am. 97(5), Pt. 2, 3387 (May 1995).

2. D. Yelton and M. Stern, "A numerical investigation of the relative scattering of Biot fast and slow waves by a spherical inclusion in a poroelastic medium," J. Acoust. Soc. Am. 98(5) Pt. 2, 2972 (November 1995).

An acoustic model of a laminar sand bed

Nicholas P. Chotiros, Dennis J. Yelton

Applied Research Laboratories, The University of Texas at Austin, Austin, Texas 78713-8029

and Morris Stern

Dept. of Aerospace Engineering and Engineering Mechanics, The University of Texas at Austin, Austin, Texas 78712

Abstract

It is postulated that a laminar sand bed may be modeled as an ensemble of randomly layered poroelastic material. The thickness of each layer was related to the associated grain size and porosity by a conservation of mass relationship. The effect of lateral variations in grain size were simulated by performing a coherent ensemble average of results from several realizations of the randomly stratified medium. Poroelastic medium parameters were chosen to represent water-saturated sand. The mean and standard deviation of the grain size distribution were chosen to match existing experimental data. Specifically, the sand bed was modeled as bounded by a homogeneous water halfspace above, and a homogeneous poroelastic halfspace of equivalent average porosity below. Reflected and transmitted signals were computed. Coherent and random components of the reflected signal were calculated. The coherent parts were directly related to the reflected and the transmitted waves. Results show significant differences between the modeled sand bed and an equivalent uniform Biot medium. The fast wave attenuation shows strong anisotropy. The slow wave is only detectable in the sand bed at shallow grazing angles.

I. INTRODUCTION

The goal of this study was to investigate the extent to which sediment granularity and bedding can influence sound propagation in ocean sediments, particularly water-saturated sand. Typically, a couple of devices are employed to match theory to experimental measurements of attenuation and scattering -- the attenuation is accounted for in terms of a complex bulk modulus, and the scattering is modeled as a random field of point scatterers in which the scattering strength is adjusted to match the measured data. Both devices have very little physical basis. Our hypothesis is that both attenuation and scattering might be explained in terms of acoustic interaction with structures associated with granularity and bedding. The viscoelastic theory of acoustic propagation in a solid is not a suitable starting point since it does not possess a mechanism that can account for the interaction between pore fluid and solid particles. Our starting is Biot's theory of acoustic propagation in a poroelastic medium. It contains the basic mechanisms of acoustic interaction between the solid matrix and pore liquid as far as forward propagation is concerned, but it does not have any mechanism to account for scattering and any associated losses. In this study, Biot's theory is extended to include the effects of granularity and bedding, used a brute force, numerical simulation approach.

II. BACKGROUND

Current models of acoustic bottom backscatter from sandy sediments are based on composite roughness and volume scattering effects from sediments modeled as fluids.[1,2] However, recent bottom penetration experiments by Chotiros[3,4] have shown that Biot's theory[5,6] of sound propagation through a fluid-filled porous solid matrix better explains the refraction of acoustic energy into the sediment. Biot's theory treats acoustic propagation through a poroelastic medium as a coupled wave motion within the solid and the pore fluid. The medium is modeled as a solid with tubular pores, as illustrated in Fig. 1. The propagating wave, in the direction of the pore tubes, can be decomposed into three components -- a fast and slow compression wave, and a shear wave. The equations of motion, in a form used by Stern, Bedford, and Millwater[7] (correcting for typographical errors), are

$$\mu \nabla^2 \mathbf{u} + (H - \mu)\nabla(\nabla \cdot \mathbf{u}) - C\nabla(\nabla \cdot \mathbf{w}) = \rho \ddot{\mathbf{u}} - \rho_f \ddot{\mathbf{w}} \qquad (1)$$

$$C\nabla(\nabla \cdot \mathbf{u}) - M\nabla(\nabla \cdot \mathbf{w}) = \rho_f \ddot{\mathbf{u}} - \frac{c\rho_f}{\beta}\ddot{\mathbf{w}} - \frac{F^* \eta}{\kappa}\dot{\mathbf{w}} \qquad (2)$$

where $\mathbf{u}$ is the displacement vector of the solid frame, $\mathbf{w}$ is the negative porosity times the displacement vector of the pore fluid relative to the solid frame, β is the porosity of the solid frame, ρ_f is the mass density of the pore fluid, ρ is the mass density of the saturated sediment, μ is the shear modulus of the solid frame, c is the virtual mass coefficient of fluid motion, η is the viscosity of the fluid, and κ is the permeability of the solid frame. C, H, and M, are constitutive coefficients depending on β, μ, and the bulk moduli of the pore fluid, grain material, and the saturated sediment. F is a frequency-dependent dynamic correction term describing the frictional force due to the relative motion of the solid and fluid, as defined by Biot.[7] The relationships between the parameters of Equations (1) and (2) are given in Appendix A. In reality the pores are significantly more tortuous and twisted than the ideal, colinear tubular structures upon which the model is based. These deviations from the ideal are accounted for in the permeability and virtual mass terms, κ and c, respectively, as drag and inertia. These terms, in combination with the log decrement terms, allow the model to represent the macroscopic forward propagation of acoustic waves in a wide range of porous media. However, the theory has no mechanism for scattering because the pores are modeled as parallel smooth walled tubes, perfectly aligned with the direction of wave propagation.

When $\mathbf{u}$ and $\mathbf{w}$ are written in terms of vector and scalar potentials, the above two equations separate into four coupled vector partial differential equations. For homogeneous media, the vector and scalar potentials have plane wave solutions. At a fluid/poroelastic interface, there are four boundary conditions imposed on these solutions -- continuity of fluid pressure, continuity of shear traction, continuity of normal traction, and continuity of normal fluid displacement. At a poroelastic/poroelastic interface there are two additional boundary conditions -- continuity of tangential solid displacement and continuity of normal solid displacement. The mathematical formulation of the differential equations and boundary conditions governing the vector and scalar potentials are illustrated by Stern, Bedford, and Millwater,[7] and outlined in Appendix A.

III. MODEL

A. Granular medium

The term "poroelastic" refers to a medium that follows Biot's theory of acoustic propagation as described by Equations (1) and (2), in which the pores are initially modeled as parallel tubes as described in Fig. 1. However, since the underlying tubular structure is colinear with the direction of wave propagation, it is unable to model the effects of pore size variations that are undoubtedly present in granular sediments.

In the context of this study, the term "granular" refers to a medium that is more complicated than the poroelastic medium as defined in Biot's theory. In the granular medium, the local pore size may vary as a function of position, leading to variations in porosity, permeability and virtual mass constant. These variations produce local changes in impedance and sound speed which interact with propagating waves. This may be illustrated in the case of a tetrahedral lattice of spherical grains, a cross-section of which is shown in Fig. 2(a). It is apparent that the local pore area in any vertical cross-section is dependent on the vertical distance z. In this example, the local porosity in the plane AA is evidently less than that in the plane BB. The porosity varies periodically as a function of z as indicated in the graph. The period d_k is a little less than the grain diameter a.

Biot's equations were not intended to account for the effects of the local porosity variations. It is implicit that the tubular pores have constant cross-section, although it is recognized that they represent a more complicated structure. The acoustic characteristics of local porosity variations, if any exist, will not be found in Biot's equations. The underlying hypothesis in this study is that these local porosity variations play a significant role in both attenuation and scattering of acoustic waves, and therefore, there is a need to model them. Two approaches are possible. On the one hand, one can start at the microscopic level, and construct a very detailed finite element model and work up towards the total acoustic response. This approach promises to be computationally intensive even if the physics of grain-grain and grain-fluid interactions were understood, which they are not. On the other hand, one can start at the

4

macroscopic level with Biot's equation, and extend it to include local variations, in steps of increasing complexity. The latter is the adopted approach.

"Bedding" is a term that is used to describe the structure of a sediment. It is the product of different combinations of grain size, shape, orientation and packing.[8] Let us assume that the local structure of a sand bed may be divided into distinct layers. Each layer being approximately one grain diameter thick, and termed a "monolayer." The regular lattice structure in Fig. 2(a) certainly fits this description, where "k" is the number of the monolayer. Laminated bedding, characterized by very fine stratification and moderately common in occurrence, may be approximately described as a series of randomly varying monolayers. Crossbedding, characterized by regions of laminar bedding of varying orientations, may be similarly described but on a local scale. Other types of bedding, such as massive bedding, are unlikely to fit this description and are excluded from this study.

Within a monolayer, the pore area changes through one complete cycle, as shown in Fig. 2(a). Let us approximate the pore area variation as a periodic two-step cycle, as illustrated in Fig. 2(b). Within each step the medium is modeled as a uniform Biot medium. The boundary between adjacent steps must satisfy all the boundary conditions between two Biot media. In principle, the period, mean and standard deviation of the variations may be matched to that of any laminar bedding. The propagation of sound through such a medium may be computed using an adaptation of Biot's equations for stratified media.

It is expected that the sound field in a sandy sediment may be considered in terms of a deterministic or coherent component, and a random or incoherent component resulting from variations in the acoustic properties as a function of position. In the case of laminar or cross bedding, the randomness is expected to be governed by a spatial correlation function that is wide in the horizontal dimensions, but as narrow as a monolayer thickness in the vertical dimension. On a local scale, the sound field may be modeled as a randomly stratified Biot medium. On a macroscopic scale, the statistics of the sound field, i.e., mean and standard deviation of acoustic pressure, may be generated numerically by taking the sum of several realizations of a randomly layered Biot medium.

B. Sand

The model has two critical components, the probabilistic definition of the layered structure and the solution of the wave propagation problem through numerous layers. The model is fashioned after the sand samples used in Nolle's measurements, which had a mean porosity of 36%.

Referring to Fig. 2(a), for a 36% porosity the mean monolayer thickness is 0.688a. Setting the thickness of each Biot layer to be exactly half of that of the monolayer,

$$h_i = 0.344a \tag{3}$$

In general, the grain diameter a, in meters, is not a constant, but a random variable. The distribution of the log of the grain diameter is usually approximated by a normal distribution.

The porosity β_k of the Biot layers alternates between two nominal values, as illustrated in Fig. 2(b). The lattice spacing of the tetrahedral structure in Fig. 2(a) may be adjusted to give any arbitrary value of mean porosity μ_β. For a mean porosity of 36%, the standard deviation σ_β was computed to be 14.5%.

Going from a tetrahedral structure to a random, close-packed structure, a degree of randomness must be introduced into the porosity. Measurements by Finney and Wallace[9] indicate that the pore volume distribution may be approximated by a log-normal distribution with a standard deviation of 0.6 Nepers. Thus, the porosity of the Biot layers is modeled as,

$$\beta_k = (\mu_\beta + (-1)^k \sigma_\beta)\, b \tag{4}$$

where the log of b follows a normal distribution with a mean value of zero, and a standard deviation of 0.6 Nepers.

C. Reflection and propagation

In modeling the propagation of a sound wave, in water, incident on a sand bed, and the subsequent reflection and transmission, consider a sand bed

sandwiched between an upper half-space of water and lower half-space of a uniform Biot medium, as illustrated in Fig. 3. Both the sand bed and the lower half-space are saturated with water. The lower half-space is a uniform Biot medium in which the parameter values are set equal to the average parameter values in the sand bed. The incident sound wave from the water would be partially reflected at the water-sand bed interface, and transmitted into the sand bed as fast, slow and shear waves. At the lower interface, there will be transmission into the lower half-space, and perhaps further reflection back into the sand bed. Of particular interest is the reflected wave at the water-sand bed interface and the transmitted waves into the lower half-space. Ideally, if the granularity of the sand bed has negligible effect on the propagating waves, then, the sand bed would be indistinguishable from the Biot medium in the lower half-space, and the water-sand bed interface would be the only interface of any significance.

The lateral variations of the sand bed need to be taken into account. A locally stratified medium is assumed with a lateral correlation length r_c, as illustrated in Fig. 3. The granular structure is assumed to be horizontally stratified within the correlation length. On a local scale, the reflection coefficient R and transmission coefficients T_f, T_s, and T_t of the fast, slow and shear waves, respectively, are predicted by the solution of Equations (1) and (2) for a randomly stratified medium, which will be described in the following section.

Of particular interest is the macroscopic sound field, both in the water and in the substrate. If the surface of the sand were rough, the roughness would need to be taken into consideration, but in this study, for simplicity, the surface roughness of the sand bed will be assumed to be negligible. Second, the Kirchhoff approximation is assumed, i.e., the local reflection and transmission coefficients are assumed to be equal to that of an infinite medium with the same horizontal stratification. Therefore, the correlation length r_c, must be large compared to a wavelength, at the very least.

On a macroscopic scale, the coherent or average reflection coefficient R_a for plane waves is simply equal to the average of all the local reflection coefficients. Similarly, for the coherent transmission coefficients T_{fa}, T_{sa}, and T_{ta}, for shallow depths of penetration.

7

$$R_a = <R> \tag{5}$$
$$T_{fa} = <T_f> \tag{6}$$
$$T_{sa} = <T_s> \tag{7}$$
$$T_{ta} = <T_t> \tag{8}$$

Therefore, the coherent reflection and transmission coefficients may be numerically computed as the simple average of several realizations of a randomly stratified Biot medium.

The result is a randomized, layered Biot medium which, to some extent, simulates the acoustic behavior of a laminar sand bed for the purpose of modeling the propagation and attenuation of acoustic waves.

D. Implementation

To implement the model, a numerical process for computing the reflection coefficient of a finely layered medium was developed, based on the interface boundary equations as defined by Stern, Bedford, and Millwater.[7] At a fluid-to-Biot medium interface, there are four boundary conditions that must be satisfied. At each interface between adjacent Biot layers there are six boundary conditions. Therefore, to model an n-layer medium would require solving a (6n+4) by (6n+4) banded matrix equation. Using this approach it was quickly found that problems with more than a few hundred layers would became impractical due to the enormous computer time required. A different method was found that greatly reduce computation resource requirements. It was found that the (6n+4) by (6n+4) banded matrix was reducible to a 4x4 matrix calculation of the form

$$(M \mid Q) x = b , \tag{9}$$

where the 4x4 matrix ($M \mid Q$) consists of a 4x1 matrix M, which depends solely on the properties of the semi-infinite fluid overlayer, augmented with a 4x3 matrix Q, which is the product of three matrices: a 4x6 prefix matrix P that is independent of fluid, sediment, or semi-infinite Biot layer properties, a 6x6 matrix S_N that depends solely on the layered sediment properties, and a 6x3 matrix C that depends solely on the semi-infinite Biot layer properties. The

8

4-vector **x** contains the solution for the reflection coefficient and the transmission coefficients through the multi-layered sediment for the Biot fast, slow, and shear waves. The 4-vector **b** depends solely on the properties of the fluid overlayer. Since S_N contains all the layered sediment information, the problem reduces largely to studying the properties of this matrix. It has the following simple form,

$$S_N = L_1 L_2 \dots L_N \tag{10}$$

where the 6x6 matrix L_i depends solely on the properties of the ith sediment layer. L_i in turn, is defined as,

$$L_i = B_i D_i^{-1} B_i^{-1}, \tag{11}$$

where the 6x6 matrix B_i depends solely on the material properties of the ith Biot layer and D_i is a diagonal 6x6 matrix depending on both the material properties and the layer thickness. Details are provided in Appendix B.

IV. MODELING OF WATER SATURATED SAND

Of particular interest was the modeling of water-saturated sand, because the sediment in many shallow water regions at the periphery of the oceans is sandy. The average Biot parameters were obtained using a procedure by Chotiros[4]. In addition, the distribution functions of the grain sizes were needed. The modeling effort was directed towards samples of well-sorted quartz sand used by Nolle et al.[10] There were four different samples. In each sample, the grain size distribution, as shown in Fig. 1 of reference [10], may be approximated by a log-normal distribution. The log-normal approximation permits the statistics of the grain size to be represented by just two parameters, mean and standard deviation. The actual values are shown in Table 1. Finally, the frame moduli and log decrements were adjusted to give reflection loss, and fast wave speed and attenuation that agreed with the measurements by Nolle, at 500 kHz. The final set of parameter values is as shown in Table 2.

A. Reflection

Reflection loss was computed as a function of the number of layers. One realization as a function of increasing sand bed thickness (or number of random layers), for sand sample #1, is shown in Fig. 4. Initially, the reflection coefficient varied wildly with the addition of each new layer due to interference effects caused by multiple scattering within the layered medium and its boundaries. As the number of layers steadily increased, the amplitude of the reflected signal appeared to converge towards an asymptotic value. A point is reached, at about 600 layers, beyond which additional layers have insignificant effect.

Using 1000 layers, the normal incidence reflection coefficient of several realizations of the randomly stratified medium were computed. The computations were made for a an acoustic frequency of 500 kHz. In each case, the mean and standard deviation were measured from ten random realizations. The mean represents the coherent part, and the standard deviation the incoherent part, of the reflection from the sand bed. The result for sample #1 is shown in Fig. 5. There is some oscillation of the coherent component at very small thicknesses, followed by a convergence towards an asymptotic value. The incoherent component is about 10 dB below the coherent component. Similar results were obtained from the simulations of the remaining three sand samples. The magnitude of the reflection coefficient is in the region of -11 dB, consistent with experimental measurements by Nolle et al.[8]. The magnitude of the asymptotic reflection coefficient as a function of grazing angles, computed for all four sand samples, are shown in Fig. 6. Compared to the predicted reflection loss from a uniform Biot medium with the same average parameter values, they are in approximate agreement. The spread is likely due the relatively small number of random realizations used to compute the mean.

B. Transmission

In addition to the reflection coefficient at the water-sand bed interface, the pressure levels of the fast, slow and shear waves transmitted into the Biot substrate was also measured. If the sand bed were a perfectly uniform Biot medium, it would be indistinguishable from the substrate, and the fast and slow wave pressure levels, as a function of bed thickness, would be expected to decrease exponentially. The rate of decay of the slow wave would be greater

due to its greater attenuation coefficient. The result for normal incidence would be as shown in Fig. 7, which was computed using the same computer code as the layered medium, but with the Biot parameters in all layers set equal to that of the substrate. At normal incidence there is no shear wave generation. Modeling the sand bed as an ensemble of randomly layered Biot media, again at normal incidence, quite a different result was obtained, as shown in Fig. 8. It appears that the slow wave pressure level transmitted into the substrate goes through a number of oscillations in the first 20 mm, and then settles down to a decay rate that is identical to that of the fast wave. An analysis of the phase rate of the slow and fast waves as a function of sand bed thickness showed that the energy that was transmitted into the substrate in the form of a slow wave had traveled through the sand bed at the speed of, not the slow wave, but the fast wave, at approximately 1700 m/s. Therefore, it must be concluded that the slow wave that was launched at the water-sand bed interface was short lived, probably going no further than the first couple of oscillations of the slow wave pressure level curve in Fig. 8. Effectively, all the energy propagating through the sand bed traveled at the fast wave speed. At the sand bed-substrate interface, part of this energy was converted into slow wave and transmitted into the substrate. This phenomenon may account for the failure of all attempts to detect the slow wave in water saturated sand by direct transmission at normal incidence, over distances greater than about a centimeter.

A similar computation at a grazing angle of 10°, which is well below the critical grazing angle of the fast wave, produced quite the opposite result. The Shear wave level was insignificant due to the extremely high attenuation at the chosen frequency. The pressure levels of the fast and slow waves transmitted into the Biot substrate are shown in Fig. 9. It shows that, beyond the evanescent layer, the fast wave level dropped rapidly and then decayed at the same rate as the slow wave. Analysis of the phase rates as a function of the sand bed thickness indicated that the energy, in both waves, traveled through the sand bed at the slow wave speed, at approximately 1000 m/s. This result is quite the opposite of that obtained at normal incidence.

The speed at which acoustic energy travels through the sand bed into the substrate, for each type of wave, is a very useful indicator of the wave propagation mechanism within the sand bed. The results for the fast, slow and

11

shear waves as a function of grazing angle are shown in Fig. 10. For the fast wave, it is seen that the effective speed through the sand bed is indeed the speed of the fast wave for grazing angles greater than 40°. Below this grazing angle, the energy that appears as the fast wave in the substrate actually travels through the sand bed at the slow wave speed. In the case of the slow wave, it is seen that at 90°, the energy that is transmitted into the substrate as a slow wave traveled through the sand bed at the speed of the fast wave. At shallow grazing angles, the slow wave energy does indeed travel through the sand bed at the slow wave speed. The apparent decrease in slow wave speed with increasing grazing angle is unexplained, as yet. For the shear wave, in only a few cases does the energy travel through the sand bed at the shear wave speed; the shear wave energy is delivered at the speed of the fast wave above 40°, or at the speed of the slow wave at lower angles.

C. Attenuation

The attenuation coefficient of waves traveling through the sand bed were computed, wherever the indicated speed matched that of the corresponding wave type. The values are compared with that of a uniform Biot medium of the same average properties. The results are shown in Fig. 11. The fast wave attenuation is found to be at a minimum at normal incidence, with values comparable to those of the uniform Biot medium, and increases quite noticeably as the grazing angle is reduced, indicating that the medium is anisotropic. The slow wave attenuation is relatively insensitive to the grazing angle, but it is significantly higher than that of the uniform medium, indicating that the random layering has caused an increase in the attenuation. The shear wave attenuation is much lower than that of the uniform Biot medium, which is predicted, at 500 kHz, to range from 21,000 dB/m for sample #1 to 8000 dB/m for sample #4. The values found were all less than 2000 dB/m. Since there were very few data points of shear wave attenuation, these results should be taken as very preliminary.

V. CONCLUSIONS

The Biot model has been extended to include the effects of granularity in a sand bed by a numerical simulation. A laminar sand bed has been treated as homogeneous Biot layers on the order of a grain diameter thick with variable

local porosity. The variations contained both deterministic and random components. Within each layer, conservation of grain volume dictates a linear relationship between the layer thickness, porosity, and grain diameter.

The effects of lateral variations in sediment structure on the mean sound field were simulated by coherently averaging the results for several random realizations. The reflection loss predicted by this model was found to be in good agreement with measured values by Nolle. The attenuation of the fast wave was found to be anisotropic. It was a minimum at normal incidence. The attenuation of the slow wave was relatively insensitive to grazing angle, but elevated relative to that of the equivalent uniform Biot medium, indicating that the granular structure has a strong effect on the slow wave.

The approach that we have taken is based on sound physical principles. It is a significant extension of Biot's theory of acoustic propagation in porous media, and gives an insight to the processes that give rise to reflection and propagation from a granular medium such as water saturated sand, that is directly applicable to ocean sediments. Follow on work will include computation of the monostatic and bistatic scattering strengths.

ACKNOWLEDGMENTS

APPENDIX A: PROBLEM SETUP AND SOLUTION

Most of the equations used are the same as those given by Stern, Bedford, and Millwater.[11] There are a few typographical errors in the equations from this reference, which have been corrected. The corrected equations in this appendix are Equations (5A), (6A), (29A), (45A), and (46A).

The ocean sediment is represented as a finite granular medium bounded above by a homogeneous fluid halfspace (water) and below by a homogeneous Biot halfspace. The granular medium is composed of homogeneous Biot layers of differing properties and thicknesses, as depicted in Fig. 3.

The layers of the finite granular medium are numbered 1 to N, from top to bottom. The homogeneous Biot halfspace is layer number $N + 1$, and the fluid medium is number 0. All $N + 1$ Biot layers have identical values for the fluid viscosity (η), fluid mass density(ρ_f), fluid bulk modulus (K_f), grain mass density (ρ_g), grain bulk modulus (K_r), frame shear modulus (μ_0), and frame bulk modulus (K_{b0}). The fluid medium has the same fluid mass density(ρ_f) and fluid bulk modulus (K_f) as the Biot media. These values are given in Table 1.

The ith layer of the granular medium corresponds to a monolayer of granular material of uniform, but randomly chosen, grain size, a_i. The choice of a grain size distribution is the sole free parameter for generating a granular sediment of given total thickness.

In this model there is a correlation between the thickness, h_i, and porosity, β_i, of the ith layer within the granular medium. Each layer represents a <u>monolayer</u> of granular material of uniform grain size. So for a given grain size, greater layer thickness implies greater fluid volume within the layer, and hence greater porosity for the layer. For a given grain size distribution, the dimensionless layer thickness distribution is identical to that of the grain size distribution. The mean of the layer thickness distribution is chosen so that average porosity of a many-layered granular medium would be the same as for the homogeneous Biot halfspace, β_{N+1}. The porosity of the ith layer is simply the

ratio of the fluid volume to the total volume of the layer. Due to the effectively one dimensional character of the simulations in this present study, we chose

$$\beta_i = 1 - \frac{a_i}{h_i}, \qquad i = 1, 2, ..., N, \tag{1A}$$

$$\beta_{N+1} = 0.36. \tag{2A}$$

The skeletal frame's bulk and shear logarithmic decrements are set equal to zero for the first N layers, and set equal to 0.15 for the final semi-infinite layer.

$$\delta_i = \delta_{si} = 0, \qquad i = 1, 2, ..., N, \tag{3A}$$

$$\delta_{N+1} = \delta_{sN+1} = 0.15, \tag{4A}$$

$$K_{bi} = K_{b0}\left(1 - i\frac{\delta_i}{\pi}\right), \tag{5A}$$

$$\mu_i = \mu_0\left(1 - i\frac{\delta_{si}}{\pi}\right). \tag{6A}$$

The mass density of the saturated sediment is simply

$$\rho_i = (1 - \beta_i)\rho_g + \beta_i\rho_f. \tag{7A}$$

The constitutive coefficients given in Equations (1) and (2) are

$$M_i = \frac{K_r}{1 - \frac{K_{bi}}{K_r} + \beta_i\left(\frac{K_r}{K_f} - 1\right)}, \tag{8A}$$

$$C_i = \left(1 - \frac{K_{bi}}{K_r}\right)M_i, \tag{9A}$$

$$H_i = \left(1 - \frac{K_{bi}}{K_r}\right)C_i + K_{bi} + \frac{4}{3}\mu_i. \tag{10A}$$

A plane wave of angular frequency ω is incident upon this sediment configuration from above with grazing angle θ. The component of the wavenumber parallel to the fluid/sediment interface is

$$k = \omega\sqrt{\frac{\rho_f}{K_f}}\cos(\theta), \tag{11A}$$

where ρ_f and K_f are the fluid mass density and fluid bulk modulus, as given in Table 1. The simulations of the present study concern the effectively one dimensional case of normal incidence, with $k = 0$.

For the ith layer, the virtual mass coefficient, c, and the permeability, κ, of Equation (2) are given by

$$c_i = 1 + 0.5\frac{1 - \beta_i}{\beta_i}, \tag{12A}$$

and

$$\kappa_i = \frac{\beta_i p_i^2}{20}, \tag{13A}$$

where p_i is the pore size parameter, given by

$$p_i = \frac{\beta_i a_i}{3(1 - \beta_i)}, \quad i = 1, 2, 3, ..., N, \tag{14A}$$

$$p_{N+1} = \frac{\beta_{N+1}\langle a \rangle}{3(1 - \beta_{N+1})}, \tag{15A}$$

and $<a>$ is the mean of the grain size distribution.

The dynamic correction term, F, of Equation (2), depends on the incident frequency. For the ith layer, it can be written as

$$F_i = \frac{\xi_i T(\xi_i)}{4\left[1 - \dfrac{2T(\xi_i)}{i\xi_i}\right]}, \tag{16A}$$

16

where

$$T(\xi_i) = \frac{\text{ber}'(\xi_i) + i\,\text{bei}'(\xi_i)}{\text{ber}(\xi_i) + i\,\text{bei}(\xi_i)} , \qquad (17A)$$

and

$$\xi_i = p_i \sqrt{\frac{\omega \rho_f}{\eta}} . \qquad (18A)$$

The horizontal position coordinate is denoted by x. The vertical position coordinate increases downward, and for the ith layer is denoted by z_i. At the upper boundary of the ith Biot layer, $z_i = 0$. The first vertical coordinate, z_0, within the fluid medium, is set equal to zero at the fluid/sediment interface.

The solid displacement term, $\mathbf{u}$, and the relative solid/fluid displacement term, $\mathbf{w}$, from Equations (1) and (2) can be expressed in terms of scalar and vector potentials:

$$\mathbf{u} = \nabla \Phi_s + \nabla \times \Psi_s , \qquad (19A)$$

$$\mathbf{w} = \nabla \Phi_f + \nabla \times \Psi_f . \qquad (20A)$$

The scalar and vector potentials for the ith layer can be written as

$$\Phi_{si} = \phi_{si}(z_i)\, e^{i(kx - \omega t)} , \qquad (21A)$$

$$\Phi_{fi} = \phi_{fi}(z_i)\, e^{i(kx - \omega t)} , \qquad (22A)$$

$$\Psi_{si} = \psi_{si}(z_i)\, e^{i(kx - \omega t)}\, \mathbf{j} , \qquad (23A)$$

$$\Psi_{fi} = \psi_{fi}(z_i)\, e^{i(kx - \omega t)}\, \mathbf{j} . \qquad (24A)$$

Inserting these into Biot's equations of motion, Equations (1) and (2), yields a set of four coupled equations for the ϕs and ψs:

$$\phi_{si}^{''} + v_{si}^2 \phi_{si} - \zeta_{si}^2 \phi_{fi} = 0, \tag{25A}$$

$$\phi_{fi}^{''} + \chi_{fi}^2 \phi_{fi} - \lambda_{fi}^2 \phi_{si} = 0, \tag{26A}$$

$$\psi_{si}^{''} + l_{si}^2 \psi_{si} = 0, \tag{27A}$$

$$\psi_{fi} = \gamma_i \psi_{si}, \tag{28A}$$

where

$$\alpha_i = i \frac{F_i^* \eta \omega}{\kappa_i}, \tag{29A}$$

$$\overline{\rho}_i = \frac{c_i \rho_f}{\beta_i}, \tag{30A}$$

$$\gamma_i = \frac{\rho_f \omega^2}{\overline{\rho}_i \omega^2 + \alpha_i}, \tag{31A}$$

$$d_i = M_i H_i - C_i^2, \tag{32A}$$

$$\kappa_{si}^2 = \frac{\left(M_i \rho_i - C_i \rho_f \right)}{d_i} \omega^2, \tag{33A}$$

$$\kappa_{fi}^2 = \frac{\left(H_i \overline{\rho}_i - C_i \rho_f \right)}{d_i} \omega^2, \tag{34A}$$

$$\beta_{si}^2 = \frac{\left(\rho_i - \gamma_i \rho_f \right)}{\mu_i} \omega^2, \tag{35A}$$

$$\lambda_{si}^2 = \frac{\left(M_i \rho_f - C_i \overline{\rho}_i \right)}{d_i} \omega^2, \tag{36A}$$

$$\lambda_{fi}^2 = \frac{\left(H_i \rho_f - C_i \rho_i \right)}{d_i} \omega^2, \tag{37A}$$

$$\chi_{fi}^2 = \kappa_{fi}^2 - k^2 + \frac{H_i \alpha_i}{d_i} , \qquad (38A)$$

$$\zeta_{si}^2 = \lambda_{si}^2 - \frac{C_i \alpha_i}{d_i} , \qquad (39A)$$

$$v_{si}^2 = \kappa_{si}^2 - k^2 , \qquad (40A)$$

$$l_{si}^2 = \beta_{si}^2 - k^2 . \qquad (41A)$$

The solutions to Equations (25A)-(27A) are plane waves of the form

$$\phi_{si}(z_i) = A_{+si} e^{i l_{1i} z_i} + B_{+si} e^{i l_{2i} z_i} + A_{-si} e^{-i l_{1i} z_i} + B_{-si} e^{-i l_{2i} z_i} , \qquad (42A)$$

$$\phi_{fi}(z_i) = \delta_{1i} A_{+si} e^{i l_{1i} z_i} + \delta_{2i} B_{+si} e^{i l_{2i} z_i} + \delta_{1i} A_{-si} e^{-i l_{1i} z_i} + \delta_{2i} B_{-si} e^{-i l_{2i} z_i} , \quad (43A)$$

$$\psi_{si}(z_i) = C_{+si} e^{i l_{si} z_i} + C_{-si} e^{-i l_{si} z_i} , \qquad (44A)$$

where

$$l_{1i}^2 = \frac{1}{2}\left(\chi_{fi}^2 + v_{si}^2\right) - \sqrt{\frac{1}{4}\left(\chi_{fi}^2 - v_{si}^2\right)^2 + \lambda_{fi}^2 \zeta_{si}^2} , \qquad (45A)$$

$$l_{2i}^2 = \frac{1}{2}\left(\chi_{fi}^2 + v_{si}^2\right) + \sqrt{\frac{1}{4}\left(\chi_{fi}^2 - v_{si}^2\right)^2 + \lambda_{fi}^2 \zeta_{si}^2} , \qquad (46A)$$

$$\delta_{1i} = \frac{v_{si}^2 - l_{1i}^2}{\zeta_{si}^2} , \qquad (47A)$$

$$\delta_{2i} = \frac{v_{si}^2 - l_{2i}^2}{\zeta_{si}^2} . \qquad (48A)$$

The terms l_{1i}, l_{2i}, and l_{si} are the wavenumbers of the Biot fast, slow, and shear waves within the ith layer, respectively. The "+" and "-" coefficients are the amplitudes of the downward-moving (transmitted) waves and the upward-moving (reflected) waves within the ith layer, respectively.

Let R be the reflection amplitude of the wave within the fluid medium. The unknowns of the problem are R, and the As, Bs, and Cs of Equations (42A)-(44A). Since there are no reflections within the homogeneous semi-infinite Biot medium, we have

$$A_{-sN+1} = B_{-sN+1} = C_{-sN+1} = 0. \tag{49A}$$

Thus, there are a total of $6N + 4$ unknowns, which satisfy the $6N + 4$ linear algebraic equations generated by the boundary conditions.

The boundary conditions pertain to continuity of fluid pressure, traction, fluid displacement, and solid displacement. Within the Biot media, the fluid (pore) pressure is

$$p_i = \left[M_i \left(\phi''_{fi} - k^2 \phi_{fi} \right) - C_i \left(\phi''_{si} - k^2 \phi_{si} \right) \right] e^{i(kx - \omega t)}, \ i = 1, 2, ..., N+1, \tag{50A}$$

and within the fluid medium it is

$$p_0 = \rho_f \omega^2 (1 + R) e^{i(kx - \omega t)}. \tag{51A}$$

The shear traction within the Biot media is given by

$$(\sigma_i)_{xz} = \mu_i \left[2ik\phi'_{si} - \left(\psi''_{si} + k^2 \psi_{si} \right) \right] e^{i(kx - \omega t)}, \ i = 1, 2, ..., N+1, \tag{52A}$$

and within the fluid medium it is

$$(\sigma_0)_{xz} = 0. \tag{53A}$$

The normal traction is

$$(\sigma_i)_{zz} = [H_i \left(\phi''_{si} - k^2 \phi_{si} \right) + 2ik\mu_i \left(\psi'_{si} - ik\phi_{si} \right)$$
$$- C_i \left(\phi''_{fi} - k^2 \phi_{fi} \right)] e^{i(kx - \omega t)}, \qquad i = 1, 2, ..., N+1, \tag{54A}$$

20

$$(\sigma_0)_{zz} = -p_0 = -\rho_f \omega^2 (1 + R) e^{i(kx - \omega t)}, \tag{55A}$$

and the normal fluid displacement is given by

$$(u_i)_z - (w_i)_z = \left[(\phi'_{si} + ik\psi_{si}) - (\phi'_{fi} + ik\psi_{fi})\right] e^{i(kx - \omega t)}, \tag{56A}$$
$$i = 1, 2, ..., N+1,$$

$$(u_0)_z - (w_0)_z = ik(1 - R)\tan(\theta) e^{i(kx - \omega t)}. \tag{57A}$$

Finally, within the i<u>th</u> Biot medium, the normal solid displacement is given by

$$(u_i)_z = (\phi'_{si} + ik\psi_{si}) e^{i(kx - \omega t)}, \tag{58A}$$

and the tangential solid displacement is

$$(u_i)_x = (ik\phi_{si} - \psi'_{si}) e^{i(kx - \omega t)}. \tag{59A}$$

Neither of these last two quantities have counterparts within the fluid medium.

With $h_0 = 0$, all $N + 1$ interfaces are subject to the boundary conditions

$$p_i\big|_{z_i = 0} = p_{i-1}\big|_{z_{i-1} = h_{i-1}}, \qquad i = 1, 2, ..., N+1, \tag{60A}$$

$$(\sigma_i)_{xz}\big|_{z_i = 0} = (\sigma_{i-1})_{xz}\big|_{z_{i-1} = h_{i-1}}, \qquad i = 1, 2, ..., N+1, \tag{61A}$$

$$(\sigma_i)_{zz}\big|_{z_i = 0} = (\sigma_{i-1})_{zz}\big|_{z_{i-1} = h_{i-1}}, \qquad i = 1, 2, ..., N+1, \tag{62A}$$

$$\left[(u_i)_z - (w_i)_z\right]\big|_{z_i = 0} = \left[(u_{i-1})_z - (w_{i-1})_z\right]\big|_{z_{i-1} = h_{i-1}}, \quad i = 1, 2, ..., N+1, \tag{63A}$$

and the Biot/Biot interfaces are subject to the additional two boundary conditions given by

$$(u_i)_z\big|_{z_i = 0} = (u_{i-1})_z\big|_{z_{i-1} = h_{i-1}}, \qquad i = 2, 3, ..., N+1, \tag{64A}$$

$$(u_i)_x\big|_{z_i = 0} = (u_{i-1})_x\big|_{z_{i-1} = h_{i-1}}, \qquad i = 2, 3, ..., N+1. \tag{65A}$$

21

The transmitted and reflected fast, slow, and shear wave amplitudes within each medium are determined by substituting Equations (42A), (43A), (44A), and (49A) into the above six boundary conditions and solving the resulting set of linear algebraic equations for R, and the As, Bs, and Cs.

APPENDIX B: A SIMPLE, AND VERY EFFICIENT, NUMERICAL APPROACH

The N layer problem described in Appendix A requires solving a $(6N+4) \times (6N+4)$ banded matrix equation. However, if we limit our attention to the reflection term from the sediment into the fluid, and to the transmission terms from the inhomogeneous layered sediment into the homogeneous sediment halfspace, it is possible to greatly simplify the computational complexity of the problem. The simplified approach is very computationally efficient, both in terms of memory usage and compute time, and is described below.

Given the definition of the reflection and transmission coefficients for the $i^{\underline{th}}$ layer, as displayed in Equations (42A)-(44A), we define the vectors v_i by

$$\mathbf{v}_i = \begin{pmatrix} A_{+si} \\ B_{+si} \\ C_{+si} \\ A_{-si} \\ B_{-si} \\ C_{-si} \end{pmatrix}, \quad i = 1, 2, 3, ..., N, \tag{1B}$$

$$\mathbf{v}_{N+1} = \begin{pmatrix} A_{+sN+1} \\ B_{+sN+1} \\ C_{+sN+1} \end{pmatrix}. \tag{2B}$$

The values of v_i and v_{i+1} are related by the boundary conditions supplied in Equations (60A)-(65A). These equations can be recast in matrix-vector form as

$$\mathbf{A}_i \mathbf{v}_i = \mathbf{B}_{i+1} \mathbf{v}_{i+1}, \quad i = 1, 2, 3, ..., N-1, \tag{3B}$$

$$\mathbf{A}_N \mathbf{v}_N = \mathbf{C} \mathbf{v}_{N+1}. \tag{4B}$$

where $\mathbf{A}_i$ and $\mathbf{B}_{i+1}$ are 6x6 matrices describing the boundary conditions at the lower surface of the $i^{\underline{th}}$ layer and the upper surface of the $(i+1)^{\underline{th}}$ layer, respectively, and $\mathbf{C}$ is a 6x3 matrix describing the boundary conditions at the surface of the Biot halfspace.

Applying the coordinate system described in the paragraph following Equation (18A), the matrices for the ith layer, $\mathbf{A_i}$ and $\mathbf{B_i}$, with layer thickness h_i, are related by

$$\mathbf{A_i} = \mathbf{B_i}\mathbf{D_i}, \tag{5B}$$

where

$$\mathbf{B_i} = \begin{pmatrix} \dfrac{-\Theta_{1i}\mu_i}{\omega^2} & \dfrac{-\Theta_{2i}\mu_i}{\omega^2} & \dfrac{\Pi_{si}\mu_i}{\omega^2} & \dfrac{\Theta_{1i}\mu_i}{\omega^2} & \dfrac{\Theta_{2i}\mu_i}{\omega^2} & \dfrac{\Pi_{si}\mu_i}{\omega^2} \\[2mm] \dfrac{\Omega_{1i}\mu_i}{\omega^2} & \dfrac{\Omega_{2i}\mu_i}{\omega^2} & \dfrac{-\Theta_{si}\mu_i}{\omega^2} & \dfrac{\Omega_{1i}\mu_i}{\omega^2} & \dfrac{\Omega_{2i}\mu_i}{\omega^2} & \dfrac{\Theta_{si}\mu_i}{\omega^2} \\[2mm] i\,l_{1i}\Delta_{1i} & i\,l_{2i}\Delta_{2i} & i\,k\Gamma_i & -i\,l_{1i}\Delta_{1i} & -i\,l_{2i}\Delta_{2i} & i\,k\Gamma_i \\[2mm] \dfrac{\Pi_{1i}\Sigma_{1i}}{\omega^2} & \dfrac{\Pi_{2i}\Sigma_{2i}}{\omega^2} & 0 & \dfrac{\Pi_{1i}\Sigma_{1i}}{\omega^2} & \dfrac{\Pi_{2i}\Sigma_{2i}}{\omega^2} & 0 \\[2mm] il_{1i} & il_{2i} & ik & -il_{1i} & -il_{2i} & ik \\[1mm] ik & ik & -il_{si} & ik & ik & il_{si} \end{pmatrix}, \tag{6B}$$

$$\mathbf{D_i} = \begin{pmatrix} e^{il_{1i}h_i} & 0 & 0 & 0 & 0 & 0 \\ 0 & e^{il_{2i}h_i} & 0 & 0 & 0 & 0 \\ 0 & 0 & e^{il_{si}h_i} & 0 & 0 & 0 \\ 0 & 0 & 0 & e^{-il_{1i}h_i} & 0 & 0 \\ 0 & 0 & 0 & 0 & e^{-il_{2i}h_i} & 0 \\ 0 & 0 & 0 & 0 & 0 & e^{-il_{si}h_i} \end{pmatrix}, \tag{7B}$$

and

$$\Theta_{ij} = 2\,k\,l_{ij}, \tag{8B}$$

$$\Pi_{ij} = l_{ij}^2 - k^2, \tag{9B}$$

$$\Omega_{ij} = \left(l_{ij}^2 + k^2\right)\left(\delta_{ij}C_j - H_j\right) + 2k^2, \tag{10B}$$

$$\Delta_{ij} = 1 - \delta_{ij}, \tag{11B}$$

$$\Gamma_i = 1 - \gamma_i, \tag{12B}$$

24

$$\Sigma_{ij} = \delta_{ij} M_j + C_j, \tag{13B}$$

and where M_i, C_i, H_i, k, γ_i, I_{si}, I_{1i}, I_{2i}, δ_{1i}, and δ_{2i} are defined by Equations (8A-11A), (31A), (41A), and (45A)-(48A), respectively. Furthermore, **C** is given by

$$\mathbf{C} = \mathbf{B}_{N+1} \begin{pmatrix} 1 & 0 & 0 \\ 0 & 1 & 0 \\ 0 & 0 & 1 \\ 0 & 0 & 0 \\ 0 & 0 & 0 \\ 0 & 0 & 0 \end{pmatrix}. \tag{14B}$$

Inserting Equation (5B) into Equation (3B), and rearranging terms, produces

$$\mathbf{v}_i = \mathbf{D}_i^{-1} \mathbf{B}_i^{-1} \mathbf{B}_{i+1} \mathbf{v}_{i+1}, \quad i = 1, 2, 3, \dots, N-1. \tag{15B}$$

Applying this recursively, we have

$$\mathbf{v}_1 = \mathbf{D}_1^{-1} \mathbf{B}_1^{-1} \left[\prod_{j=2}^{N-1} \left(\mathbf{B}_j \mathbf{D}_j^{-1} \mathbf{B}_j^{-1} \right) \right] \mathbf{B}_N \mathbf{v}_N. \tag{16B}$$

Inserting Equations (4B) and (5B) gives

$$\mathbf{v}_1 = \mathbf{D}_1^{-1} \mathbf{B}_1^{-1} \left[\prod_{j=2}^{N} \left(\mathbf{B}_j \mathbf{D}_j^{-1} \mathbf{B}_j^{-1} \right) \right] \mathbf{C} \mathbf{v}_{N+1}. \tag{17B}$$

Consider the matrix

$$\mathbf{P} = \begin{pmatrix} 1 & 0 & 0 & 0 & 0 & 0 \\ 0 & 1 & 0 & 0 & 0 & 0 \\ 0 & 0 & 1 & 0 & 0 & 0 \\ 0 & 0 & 0 & 1 & 0 & 0 \end{pmatrix}. \tag{18B}$$

Note that right-multiplying this matrix by any 6x6 matrix truncates the bottom two rows of the 6x6 matrix. Thus, since the rows of $\mathbf{B_1}$, each of which corresponds to one of Equations (60A)-(65A), are ordered in the same sequence as those equations, the 4x6 matrix $\mathbf{PB_1}$ describes the four boundary conditions at the fluid/Biot interface of the first sediment layer. Hence, the boundary conditions at the fluid/Biot interface can be written as

$$RM + PB_1 v_1 = b,$$
(19B)

where R is the reflection coefficient, $\mathbf{M}$ is a 4x1 matrix depending solely on the fluid and incident wave properties, and $\mathbf{b}$ is a 4-vector which also depends solely on these properties. $\mathbf{M}$ and $\mathbf{b}$ are determined from the boundary conditions at the fluid/Biot interface, as given in Equations (60A)-(63A):

$$\mathbf{M} = \begin{pmatrix} 0 \\ \rho_f \\ i\omega\sin(\theta)\sqrt{\dfrac{\rho_f}{K_f}} \\ -\rho_f \end{pmatrix},$$
(20B)

$$\mathbf{b} = \begin{pmatrix} 0 \\ -\rho_f \\ i\omega\sin(\theta)\sqrt{\dfrac{\rho_f}{K_f}} \\ \rho_f \end{pmatrix}.$$
(21B)

Inserting Equation (17B) into Equation (19B) gives

$$RM + PS_N C v_{N+1} = b,$$
(22B)

where

$$S_N = \prod_{j=1}^{N}\left(B_j D_j^{-1} B_j^{-1}\right).$$
(23B)

Note that Equation (22B) can be rewritten as

$$\left(\mathbf{M} \mid \mathbf{PS_N C}\right) \mathbf{x} \;=\; \mathbf{b}, \tag{24B}$$

where the 4x4 matrix $\left(\mathbf{M} \mid \mathbf{PS_N C}\right)$ consists of the 4x1 matrix $\mathbf{M}$ augmented with the 4x3 matrix $\mathbf{PS_N C}$, and

$$\mathbf{x} \;=\; \begin{pmatrix} R \\ A_{+sN+1} \\ B_{+sN+1} \\ C_{+sN+1} \end{pmatrix}. \tag{25B}$$

Thus, the problem of Appendix A can be solved quite simply and efficiently by forming the 4x4 matrix $\left(\mathbf{M} \mid \mathbf{PS_N C}\right)$ and then solving for $\mathbf{x}$ in Equation (18B). When compared to the original $(6N+4)\text{x}(6N+4)$ banded matrix algorithm, with $N = 500$, this method was very fast and consistently produced the same results to 14 out of 16 significant figures. However, the advantage of this approach is not purely computational. Note that all the layered sediment information is contained in the 6x6 matrix $\mathbf{S_N}$, so the behavior of an ensemble of randomly layered sediments could, in principle, be investigated by studying the statistical properties of this matrix.

REFERENCES

1   D. R. Jackson, S. P. Winebrenner, A. Ishimaru, "Application of Composite Roughness Model to High-frequency Bottom Backscattering," J. Acoust. Soc. Am., **79**(5), 1410-1422 (1986).

2   A. N. Ivakin and Yu. P. Lysanov, "Underwater Sound Scattering by Volume Inhomogeneities of a Bottom Bounded by a Rough Surface," Sov. Phys. Acoust. **27**(3), 212-215 (1981).

3   A. Altenburg and N. P. Chotiros, "Plane-wave analysis of acoustic signals in a sandy sediment," J. Acoust. Soc. Am. 89(1), 165-170 (January 1991).

4   N. P. Chotiros, "Biot Model of Sound Propagation in Water Saturated Sand," J. Acoust. Soc. Am. **97**(1), 199-214 (1995).

5   M. A. Biot, "Theory of Propagation of Elastic Waves in a Fluid-saturated Porous Solid, I. Low-frequency Range," J. Acoust. Soc. Am. **28**, 168-178 (1956).

6   M. A. Biot, "Theory of Propagation of Elastic Waves in a Fluid-saturated Porous Solid, II. Higher Frequency Range," J. Acoust. Soc. Am. **28**, 179-191 (1956).

7   M. Stern, A. Bedford, H. R. Millwater, "Wave Reflection from a Sediment Layer with Depth Dependent Properties," J. Acoust. Soc. Am. **77**(5), 1781-1788 (1985).

8   F. J. Pettijohn, P. E. Potter, and R. Siever, <u>Sand and sandstone</u>, (Springer-Verlag, New York 1987).

9   J. L. Finney and J. Wallace, "Interstitial correlation functions; a new, sensitive characterization of non-crystalline packed structures," J. Non-Cryst. Solids 43, 165-187 (1981).

10   A. W. Nolle, W. A. Hoyer, J. F. Mifsud, W. R. Runyan, and M. B. Ward, "Acoustical Properties of Water-filled Sands," J. Acoust. Soc. Am., 35(9), 1394-1408 (1963).

11   Reference 9.

List of Figures

TUBULAR
PORES
IN A
SOLID MATRIX

u

β (u - w)

SHEAR
WAVE

SLOW
WAVE

FAST
WAVE

Figure 1.
The Biot medium: tubular pores in a solid matrix.
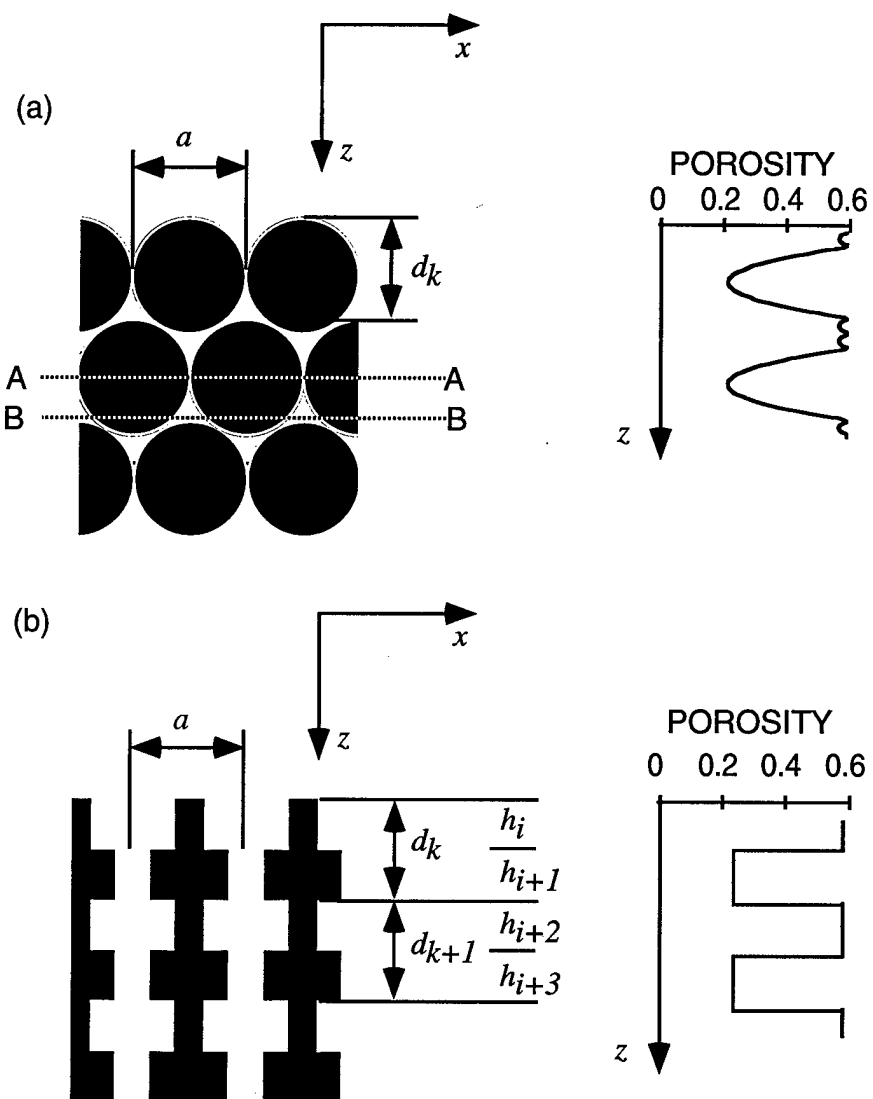
Figure 2.
Local porosity variations (a) in tetrahedral packing of spheres,
and (b) its approximation in terms of a layered Biot medium.
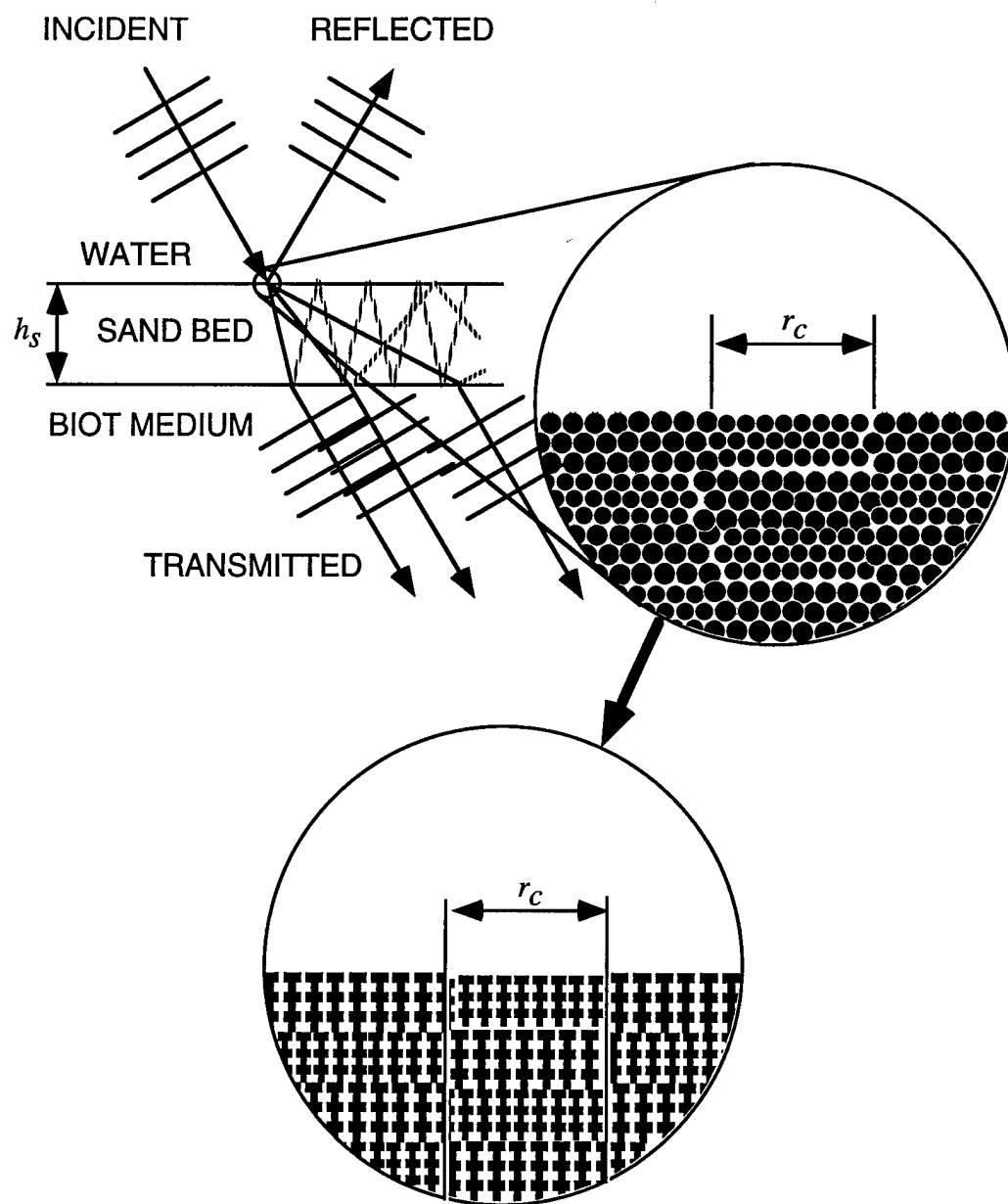
Figure 3.
Modeling of reflection and propagation through a sand bed.
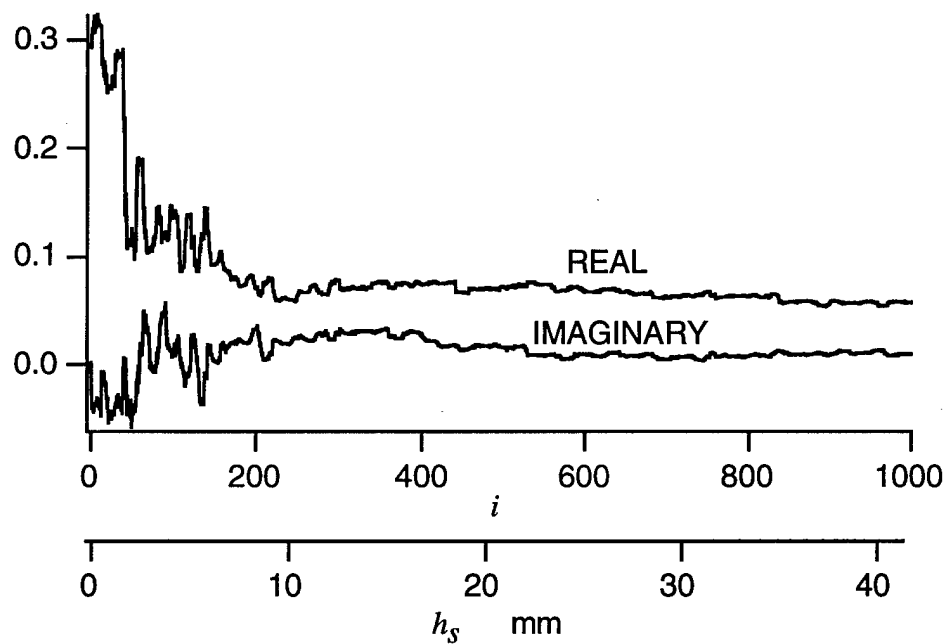
Figure 4.

Example reflection coefficient as a function of sand bed thickness
from one realization of the randomly stratified medium as a function
of sand bed thickness h_s and number of random Biot layers, i,
for sand sample #1.
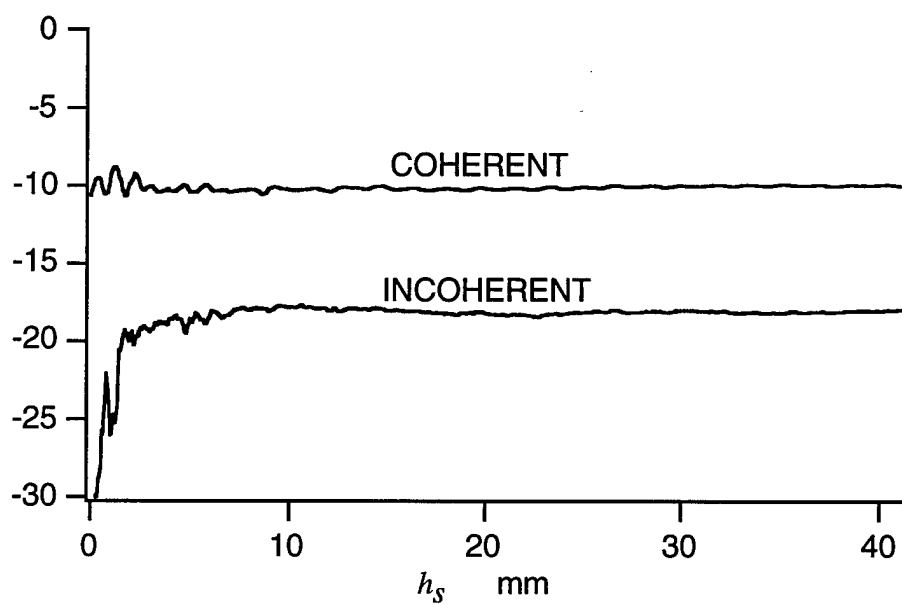
Figure 5.
Coherent and incoherent components of reflection loss
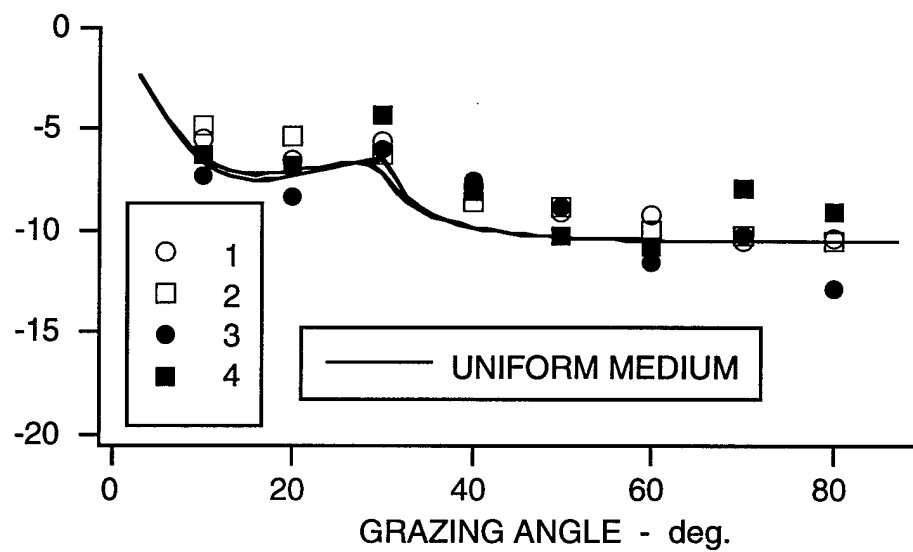as a function of sand bed thickness at normal incidence,
for sample #1.

Figure 6.

Magnitude of coherent component of reflection coefficient
as a function of grazing angle for all four sand samples,
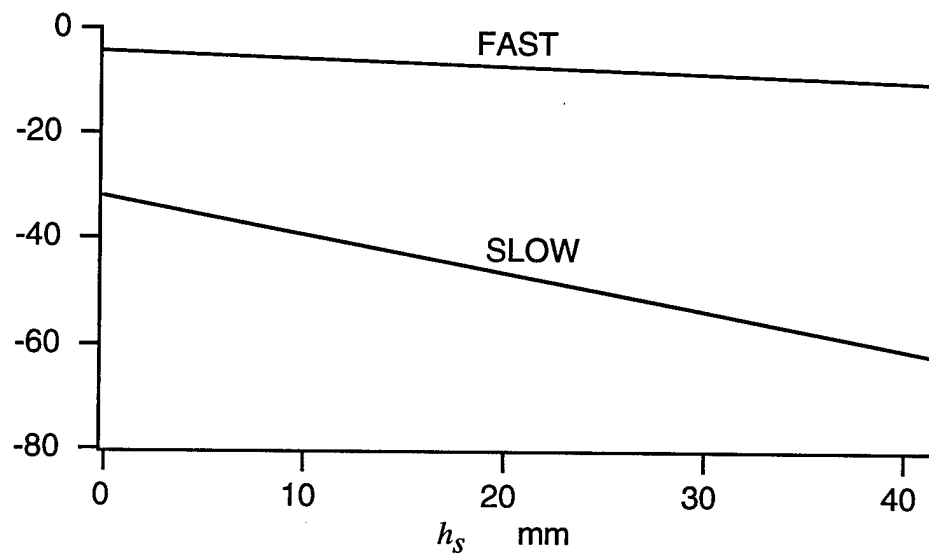and corresponding curves for a uniform Biot medium.

Figure 7.
Expected pressure levels of the fast and slow waves transmitted into the substrate as a function of sand bed thickness at normal incidence, if the sand bed were a uniform Biot medium , for sample #1.
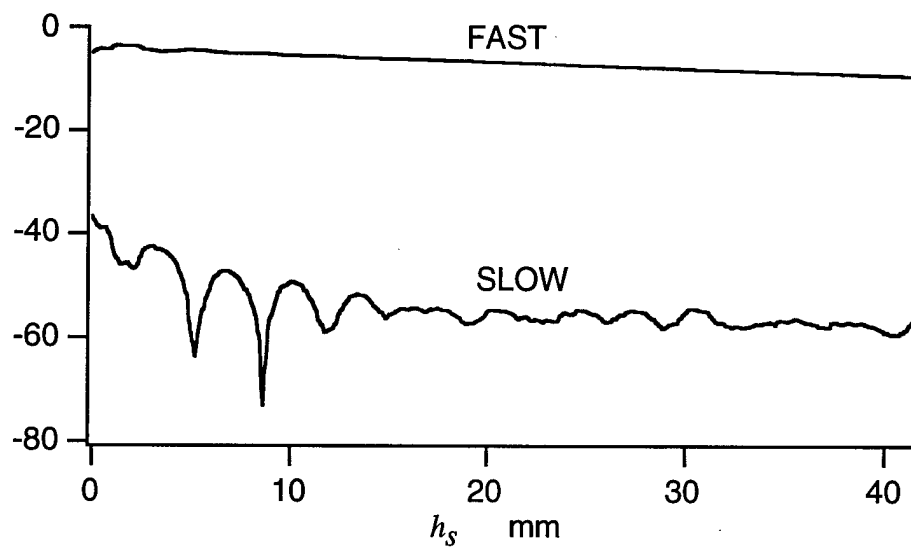
Figure 8.
Coherent components of the fast and slow waves transmitted into
the substrate as a function of sand bed thickness at normal incidence,
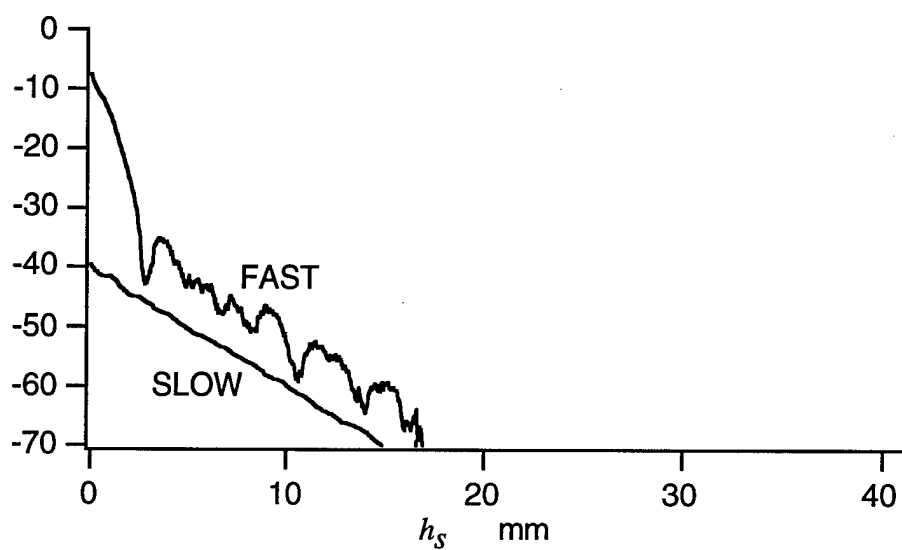and indicated wave speeds, for sample #1.

Figure 9.
Coherent components of the fast and slow waves in the substrate
as a function of sand bed thickness at 10° grazing angle, and indicated
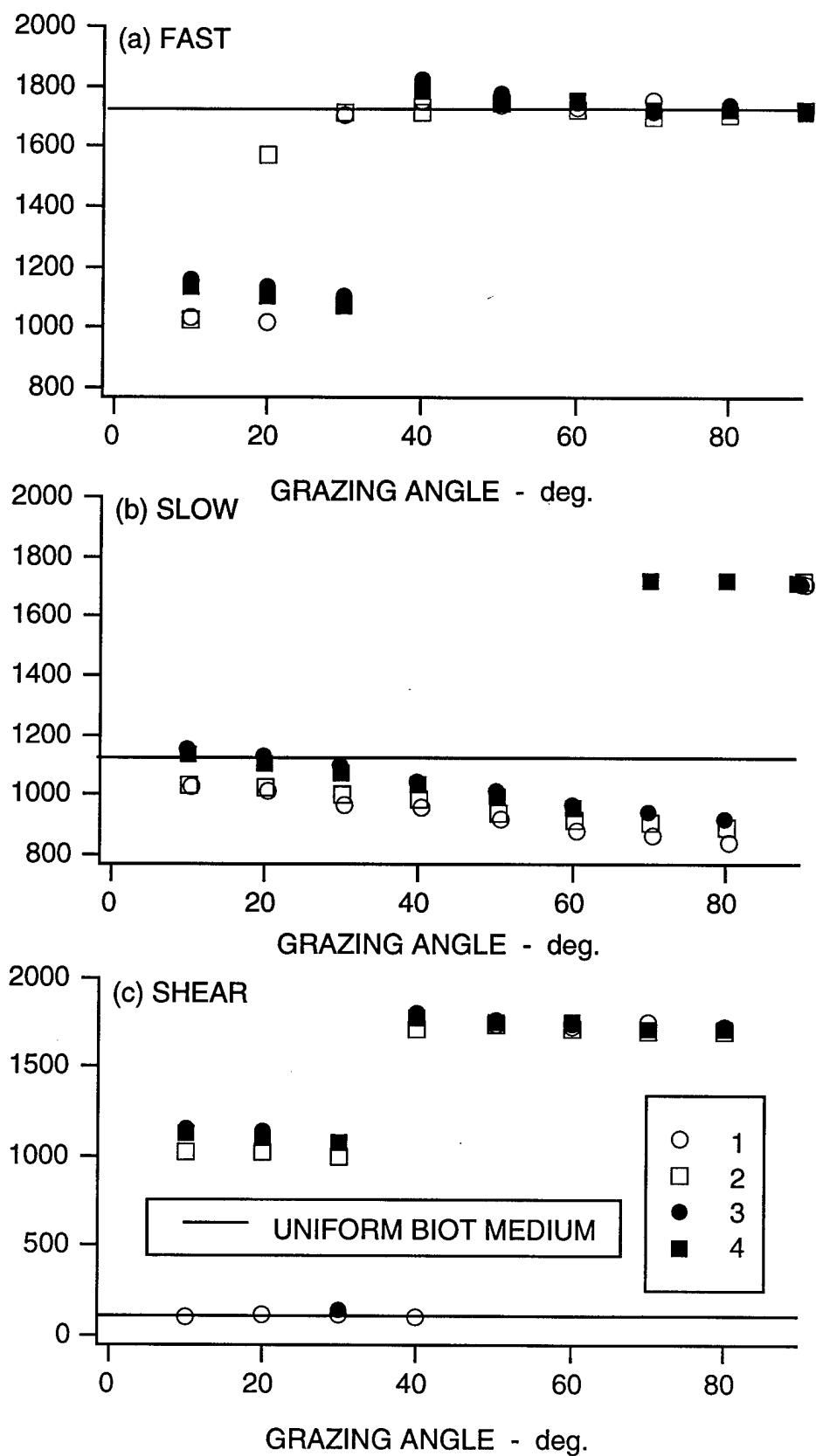wave speeds, using sample #1.

Figure 10.
Indicated transit speeds through the sand bed of (a) fast, (b) slow and (c) shear waves
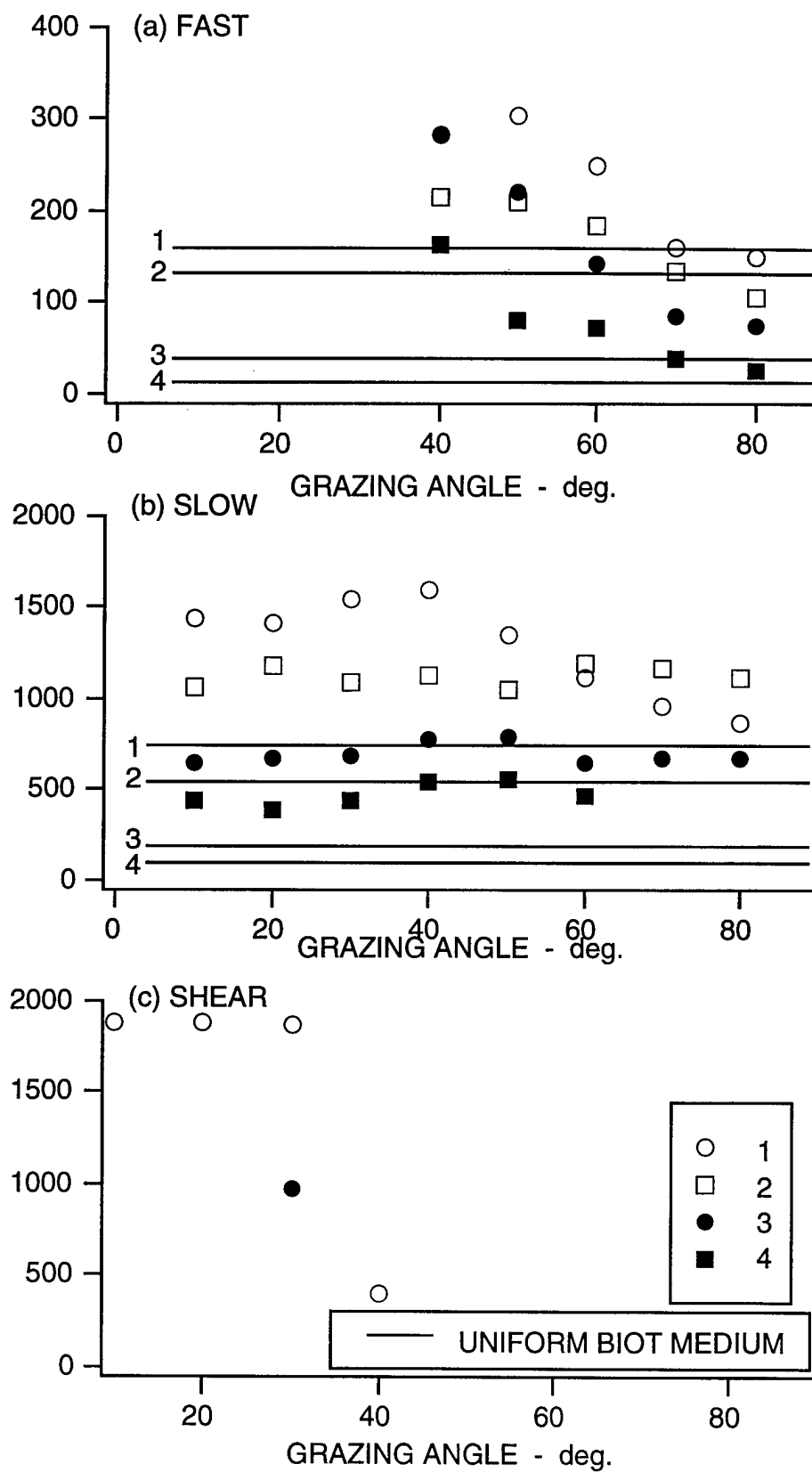transmitted into the substrate, as a function of grazing angle, computed for all sand samples.

Figure 11.
Indicated transit attenuations through the sand bed of (a) fast, (b) slow and (c) shear waves transmitted into the substrate, as a function of grazing angle, computed for all sand samples.

List of Tables

Table 1. Sand samples

Sample No.	Mesh range	mean diam. mm	stand. dev. Nepers
1	120-140	0.12	0.28
2	80-100	0.17	0.17
3	40-45	0.40	0.15
4	25-30	0.64	0.11

Table 2. Model parameters

Sample No.		1	2	3	4
From Nolle					
Reflection loss	dB	-11	-11	-11	-11
Fast wave speed	m/s	1720	1720	1720	1720
Fast wave attenuation	dB/m	17	13	6.6	4.2
Shear wave speed	m/s	100	100	100	100
Shear wave attenuation	dB/m	3000	2600	1600	1000
Average parameters					
Fluid viscosity (η)	kg/m s	0.001	0.001	0.001	0.001
Fluid mass density (ρ_f)	kg/m^3	1000	1000	1000	1000
Fluid bulk modulus (K_f)	Pa	2.25E+09	2.25E+09	2.25E+09	2.25E+09
Grain mass density (ρ_g)	kg/m^3	2650	2650	2650	2650
Grain bulk modulus (K_r)	Pa	7.00E+09	7.00E+09	7.00E+09	7.00E+09
Frame shear modulus (μ)	Pa	2.09E+07	2.08E+07	2.09E+07	2.08E+07
Frame bulk modulus (K_b)	Pa	5.60E+09	5.58E+09	5.70E+09	5.69E+09
Frame Porosity (β)	-	0.36	0.36	0.36	0.36
Frame shear log dec (δ_s)	-	0.0532	0.0459	0.0094	0.0017
Frame bulk log dec (δ)	-	0.5049	0.4402	0.2814	0.1872